

## Original Article

# Quantitative assessment of stiffness levels of hypertrophic scars in rabbit ears via shear wave elastography

Qing-Rong Yao<sup>1,2\*</sup>, Wu Tian<sup>3\*</sup>, Feng Liu<sup>2</sup>, Hong-Yong Liao<sup>2</sup>, Li Qiu<sup>1</sup>

<sup>1</sup>Department of Ultrasound, West China Hospital of Sichuan University, Chengdu, Sichuan Province, China; <sup>2</sup>Department of Ultrasound, Guizhou Provincial People's Hospital, Guiyang, Guizhou Province, China; <sup>3</sup>Department of General Surgery, Orthopedics Hospital of Guizhou Province, Guiyang, Guizhou Province, China. \*Equal contributors.

Received December 27, 2019; Accepted March 19, 2020; Epub May 15, 2020; Published May 30, 2020

**Abstract:** Purpose: The aim of the current study was to evaluate the feasibility of assisting clinical quantitative assessment of hypertrophic scars (HS) with shear wave elastography (SWE). Methods: Twelve healthy white rabbits were randomly divided into 3 groups (4 rabbits/group). Three 1.5 cm × 1.0 cm rectangle defects were created by peeling off the entire skin and perichondrium directly from the cartilage surface of the two ears of each rabbit, creating a total of 72 wounds. The specimens were cut and fixed with 4% paraformaldehyde and made into paraffin-embedded sections for hematoxylin and eosin (HE) staining, Picric acid-Sirius red staining, and CD34 immunohistochemistry. Measured data was compared with Young's modulus (including  $E_{\text{mean}}$ ,  $E_{\text{min}}$ , and  $E_{\text{max}}$ ) of the HS. Results: Histological changes of HS were consistent with the evolution of HS in the aspects of time and degrees. Microvascular density (MVD) in the hyperplasia stage was higher, compared to regression and mature stages. The percentage of type I and III collagen areas of Picric acid-Sirius red staining in the hyperplasia stage was greater than that in regression and mature stages. Changes in Young's modulus of HS were consistent with scar evolution. Young's modulus in the hyperplasia stage was significantly higher, compared to those in regression and maturity stages. Conclusion: SWE can be used to dynamically and quantitatively to evaluate stiffness levels of HS. It can be used as a reliable method, effectively assessing the evolution of HS.

**Keywords:** Shear wave elastography, hypertrophic scar, histology, ultrasound, elasticity, skin

## Introduction

Hypertrophic scars (HS) are an inevitable result of tissue repair once the skin is injured beyond a certain depth or range. When scars form, they mainly manifest as a large number of fibroblast proliferation, excessive collagen deposition [1], and neovascularization [2]. Therefore, these scars are difficult to eliminate completely.

Scar formation is a dynamic development process. Accurate assessment of HS is significant in the development of an effective treatment plan for HS. At present, there is lack of objective and effective imaging methods and quantitative indicators to evaluate HS. In clinical practice, doctors usually judge the treatment efficiency of HS subjectively, using the Vancouver scale (VSS) [3], visual analogue

scale (VAS) [4], and similarities, which can only detect external conditions of the HS, such as color, texture, toughness, and surface thickness. However, the internal structure and elasticity of HS cannot be observed and reflected. Regarding commonly used auxiliary examinations, Computerized Tomography (CT) and Magnetic Resonance Imaging (MRI) scans have poor resolution of superficial tissues, such as skin. They are often used for large and deep subcutaneous tissue, including tumors [5, 6]. Although skin biopsies are the golden standard for detection of scars [7], they are quite invasive. Thus, they cannot be used as a routine observation method.

SWE is a novel ultrasonic elasticity technology, developed in recent years. It is used to evaluate the elasticity of soft tissues. It is based on the

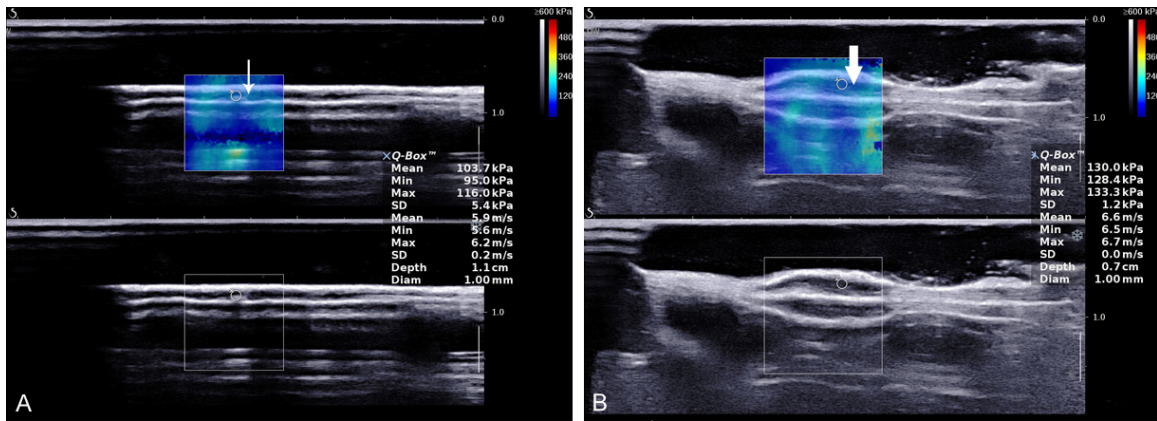


**Figure 1.** Shear wave elastography of the dermis and the corresponding elastic modulus value of the rabbit ear before operation (A); Thin arrow refers to the normal dermis layer of rabbit ear skin. The shear wave elastography and the corresponding elastic modulus value of the hyperplastic scar of rabbit ear skin (B); Thick arrow refers to the hypertrophic scar.

principle that the hardness will change, correspondingly, as tissues undergo pathological changes [8]. SWE can be used to directly measure the elasticity of tissues, indirectly reflecting the stiffness of tissues [9-11]. SWE has been widely applied in clinical research. However, it has been rarely used to study the elasticity of HS in the development process of different diseases. The purpose of the present study was to use SWE to quantitatively measure the stiffness of HS at different disease stages. Measurements were compared to pathological results, aiming to investigate the feasibility of SWE in the clinical assessment of HS.

**Materials and methods**

*Experimental setup and methods*

Twelve white rabbits, six males and six females, weighing 2.0-2.5 kg, were obtained from the Animal Institute of Guizhou Medical University. All animals were housed in an environment with a temperature of  $22 \pm 1^\circ\text{C}$ , relative humidity of  $50 \pm 1\%$ , and a light/dark cycle of 12/12 hours. All studies (including the rabbit euthanasia procedure) were carried out in compliance with Institutional Animal Care and Use Committee (IACUC) guidelines. The study protocol was approved by the Ethics Committee of Guizhou Provincial People’s Hospital.

The animals were kept in cages for one week before surgery for adaptive feeding. Twelve white rabbits were randomly divided into 3 groups (4 rabbits/group). HS models were made by adjusting the procedure reported by

Rong Yu [12]. A total of 5% compound lidocaine cream was applied to the ventral surface of the rabbit ear after barbering, then 2% lidocaine hydrochloride was injected locally for anesthetization 30 minutes later. Three 1.5 cm  $\times$  1.0 cm rectangle defects were created by peeling off the entire skin and perichondrium directly from the cartilage surface in the middle of both ears of the rabbits, creating a total of 72 wounds. Eight days after surgery, clam shells on the wound surface were removed after routine disinfection. The epidermis and granulation tissues crawling on the wound surface were scraped off. Next, the wounds were left to naturally heal after hemostasis by compression.

*Equipment and study design*

AixPlover ultrasound system (SuperSonic Imagine, Aix-en-Provence, France) with a SL15-4 linear probe, with frequencies ranging from 4 to 15 MHz, was used. First, the rabbit ear wounds were routinely scanned with the probe positioned along the long axis of the scar. The two-dimensional sonogram of the scar was observed until the structure of dermis layer was clear. Next, the shear wave elastography mode, with a range of 0~600 kPa, was adopted. The probe was left to stand for 3 to 5 seconds with no pressure applied. When the image became stable, it was frozen. The region of interest (ROI) was selected and locked in the dermis layer of the skin. The Q-Box™ Trace pattern was used to trace the lesions and measure the absolute values of Young’s modulus, including the mean, maximum, and minimum (**Figure 1A, 1B**).

After measurement by SWE, the rabbits were sacrificed by air embolisms in batches on the 30<sup>th</sup>, 60<sup>th</sup>, and 90<sup>th</sup> day after modeling, with 4 rabbits in each group. Specimens were fixed with 4% paraformaldehyde and made into paraffin-embedded sections for H&E staining, picric acid-Sirius red staining, and immunohistochemistry.

### *General observation*

Wound healing processes, including color, texture, proliferation, and degradation of the scars, were continuously observed for 3 months after modeling.

### *H&E staining*

H&E staining was carried out by a series of procedures, including dewaxing paraffin sections to water, hematoxylin staining of nucleus, eosin staining of cytoplasm, and dehydration sealing. Five view fields of 100-fold were randomly selected for each slice in each group, obtaining images. Analysis of acquired images was performed by histopathology image analysis software, Image-pro plus 6.0 (Media Cybernetics, Inc., Rockville, MD, USA).

### *Picric acid-Sirius red staining*

Picric acid-Sirius red staining was carried out by a series of procedures, including dewaxing paraffin sections to water, dying by the Sirius red staining solution, rinsing, and sealing. Five view fields of 100-fold were randomly selected for each slice in each group, obtaining images. The entire view field was filled by tissue as much as possible. Under polarized light, type I collagen was red or yellow with strong birefringence, while type III collagen was green with weak birefringence. Each photo was analyzed by Image-Pro Plus 6.0, calculating the percentage of type I and type III collagen in each area per photo.

### *Immunohistochemistry*

CD34 immunohistochemistry was conducted using various procedures, including dewaxing paraffin sections to water, antigen retrieval, blocking endogenous peroxidase, BSA or serum blocking, adding primary antibody, adding secondary antibody, DAB coloring, counterstaining nuclei, and dehydration sealing. Five

view fields of 100-fold were randomly selected for each slice in each group, obtaining images. Referring to Weidner et al., the whole slice was first examined under low-power microscopy to find three high-density areas of blood vessels, namely "hot spots". The number of blood vessels stained positively was counted under a light microscope of 200 times. The intact lumen and red blood cells are unnecessary for microvascular identification. Obviously-stained endothelial cells that were separated from adjacent blood vessels, tumor cells, and interstitial components were evaluated as independent blood vessels. Blood vessels were not clearly identified and thickness in muscle layers was not included in the count. The average number of blood vessels in 5 view fields was counted as the MVD value (/HP). Histopathology analyses of acquired images were conducted using Image-pro plus 6.0 (Media Cybernetics, Inc., Rockville, MD, USA).

### *Statistical analysis*

Descriptive statistics and inferential statistics were performed using SPSS22.0 and R language, with the significance level setting at  $P < 0.05$ . Experimental data are characterized by mean  $\pm$  standard deviation. Picric acid-Sirius red staining, MVD, and elastography data are statistically described by mean values and standard deviation. The overall trend of the above data was analyzed based on the boxplot. Multiple comparisons between groups were conducted using ANOVA, aiming to refine the relationship within each group. Spearman's correlation coefficient was used for correlation analysis and correlation testing.

## **Results**

### *Changing of the HS model of rabbit ears*

A large amount of exudation occurred in the wounds 3 days after surgery (**Figure 2A**). The wounds scabbed 8 days after surgery (**Figure 2B**). Exudation increased when the original scars and tissues were removed. However, the wounds quickly healed. By the 16<sup>th</sup> day after surgery, the wounds healed. Scar hyperplasia appeared (**Figure 2C**). In addition, scars that did not exceed the original wound surface were red in color, hard in texture, and likely to bleed when touched. Scar hyperplasia reached its



**Figure 2.** Gross specimens of hypertrophic scars in rabbit ears. 3 days postoperatively (A); 8 days postoperatively (B); 16 days postoperatively (C); 30 days postoperatively (D); 60 days postoperatively (E); 90 days postoperatively (F).

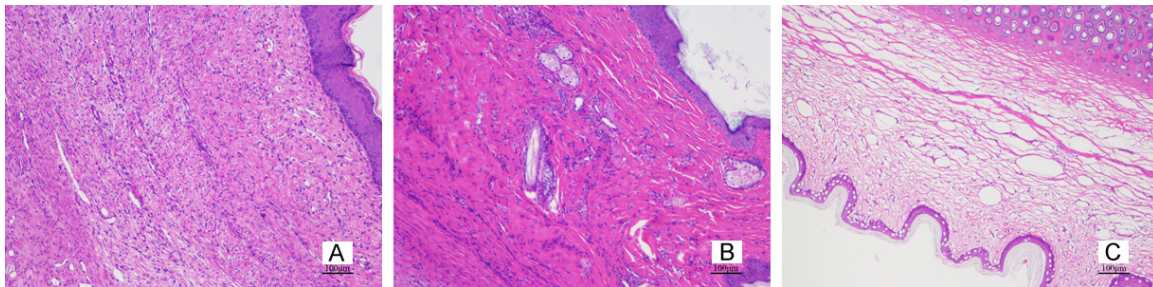


**Figure 3.** H&E staining of each time period. A. 30 days after surgery (HE × 100); B. 60 days after surgery (HE × 100); C. 90 days after surgery (HE × 100).

peak at 30 days after surgery (**Figure 2D**), featuring the papillary process in the center of the scar. By the 60<sup>th</sup> day after surgery, the color of the scars began to lighten up and the texture turned soft. However, the papillary process in the center was still obvious (**Figure 2E**). By the 90<sup>th</sup> day after surgery, the scars almost paralleled the skin, approximating the skin color with pigmentation on the surface (**Figure 2F**).

#### H&E staining results

At 30 days after modeling, cells in the dermal layer actively proliferated and many new capillaries were formed. The fibroblast proliferated and collagen fibers were disorderly arranged, with scar hyperplasia reaching a peak (**Figure 3A**). At 60 days after surgery, the scar tissues

started to fade, the number of cells in the dermis was reduced, and a large number of parallel and staggered collagen fiber bundles were seen around the cells with focal glassy degeneration (**Figure 3B**). At 90 days after surgery, the number of cells in the dermis further reduced, collagen fibers were arranged in parallel, and scars were in the mature stage (**Figure 3C**).

#### Picric acid-Sirius red staining results

A large amount of collagen was deposited in the dermis of HS by 30 days~60 days after surgery. There were many thick and dense type I collagen fibers, which were distributed in small clumps. Of these, green flocculent type III collagen fibers were observed (**Figure 4A, 4B**). The collagen content was reduced 90

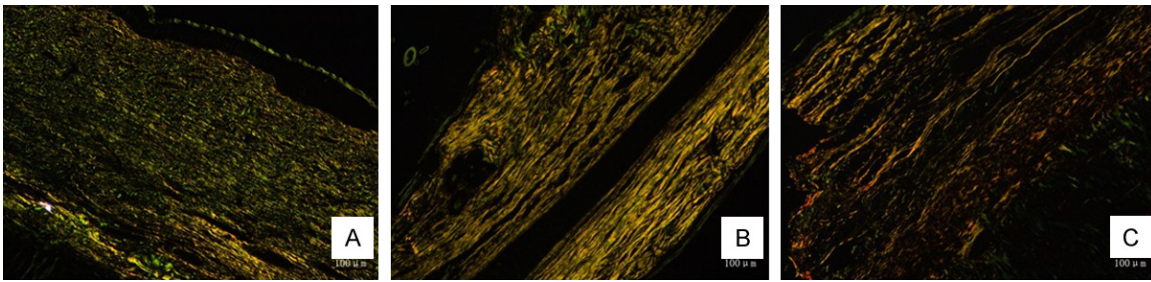


**Figure 4.** Picric acid-Sirius red stain at each time period. A. 30 days after surgery (polarized light microscope, picric acid-Sirius red staining  $\times 100$ ); B. 60 days after surgery (polarized light microscope, picric acid-Sirius red staining  $\times 100$ ); C. 90 days after surgery (polarized light microscope, picric acid-Sirius red staining  $\times 100$ ).

days after surgery and the degree of collagenous arrangement disorder was reduced (**Figure 4C**).

Type I collagen area percentages (%) at 30, 60, and 90 days after surgery were  $10.09 \pm 5.59$ ,  $11.18 \pm 5.37$ , and  $6.13 \pm 2.99$ , respectively. Type III collagen area percentages were  $11.57 \pm 4.76$ ,  $10.10 \pm 4.62$ , and  $5.17 \pm 3.41$ , respectively. The content of type I and type III collagen reached the peak between 30 days and 60 days after surgery. There were no significant differences between the two groups ( $P > 0.05$ ). At 90 days after the operation, the content of type I and type III collagen was significantly lower, compared to the content at 30 days and 60 days (**Table 1**; **Figure 5**).

#### Immunohistochemistry results

CD34 micro-vessels in immunohistochemistry decreased with the development of HS. MVD peaked at 30 days after surgery (mean = 85.72/HP). Next, it gradually decreased, reaching 77.63/HP at 60 days and 44.48/HP at 90 days (**Figures 6, 7**). Differences between 30 days and 60 days after surgery were not statistically significant ( $P > 0.05$ ), while differences between the other groups were statistically significant ( $P < 0.05$ , **Table 2**).

#### SWE analysis results

HS had different Young's modulus at different times of scar formation. Thus, Young's modulus reached a peak by 30 days after surgery. Young's modulus levels ( $E_{\text{mean}}$ ,  $E_{\text{min}}$ ,  $E_{\text{max}}$ ) were 172.10 Kpa, 155.57 Kpa, and 181.20 Kpa at 30 days after surgery. Young's modulus levels were 111.26 Kpa, 93.50 Kpa, and 131.85 Kpa at 60 days after surgery. Young's modulus levels were 75.86 Kpa, 50.19 Kpa, and 108.75 Kpa at 90 days after surgery (**Figure 8**).

Differences of  $E_{\text{max}}$  at 60 days and 90 days after surgery were not statistically significant ( $P > 0.05$ , **Table 3**), while differences between the other groups were statistically significant ( $P < 0.05$ , **Tables 4, 5**).

#### Discussion

With the rapid development of digital ultrasound technology, HFUS has become widely used for the evaluation of skin and HS [13, 14]. However, HFUS can only measure the thickness and echo changes of scars. It cannot reflect the mechanical characteristics of skin and scars. The elasticity of HS is closely related to biological properties [15]. Young's modulus values can reflect tissue elasticity, indirectly reflecting tissue hardness. Therefore, the measurement of scar elasticity is helpful for the evaluation of scars. Currently, there are three main types of ultrasound elastography used for skin and skin scars, including strain elastography (SE), acoustic radiation force impulse (ARFI), and SWE.

SE includes imaging of the compressional elastic imaging mode. The operator needs to outsource oppression patients body surfaces and identify target tissues due to different internal hardness of the stress strain, as well as focus on collection, perform analysis, organize reflection echo signals before and after the pressure difference, and present the color ultrasonography of tissue elasticity imaging through the color coding [16]. It has been reported that when SE is used to measure the elasticity of keloid skin, lesion tissues in the mature stage are soft with a large strain, while lesion tissues in the proliferative stage are hard with a small strain. Elasticity is inversely proportional to the hardness of the tissues [17]. However, this is a qualitative and semi-

## Shear wave elastography in HS

**Table 1.** Multiple comparisons and tests of differences between the Picric acid-Sirius red staining groups

	collagen I				collagen III			
	differences between groups	lower confidence limit	upper confidence limit	<i>p</i>	Differences between groups	lower confidence limit	upper confidence limit	<i>p</i>
60 days postoperatively-30 days postoperatively	2.16	-1.83	6.14	0.40	-1.78	-5.32	1.76	0.45
90 days postoperatively-30 days postoperatively	-3.89	-7.15	-0.64	0.02	-6.51	-9.4	-3.62	<0.01
90 days postoperatively-60 days postoperatively	-6.05	-10.04	-2.07	<0.01	-4.73	-8.27	-1.19	0.01

*P*<0.05 was statistically significant.

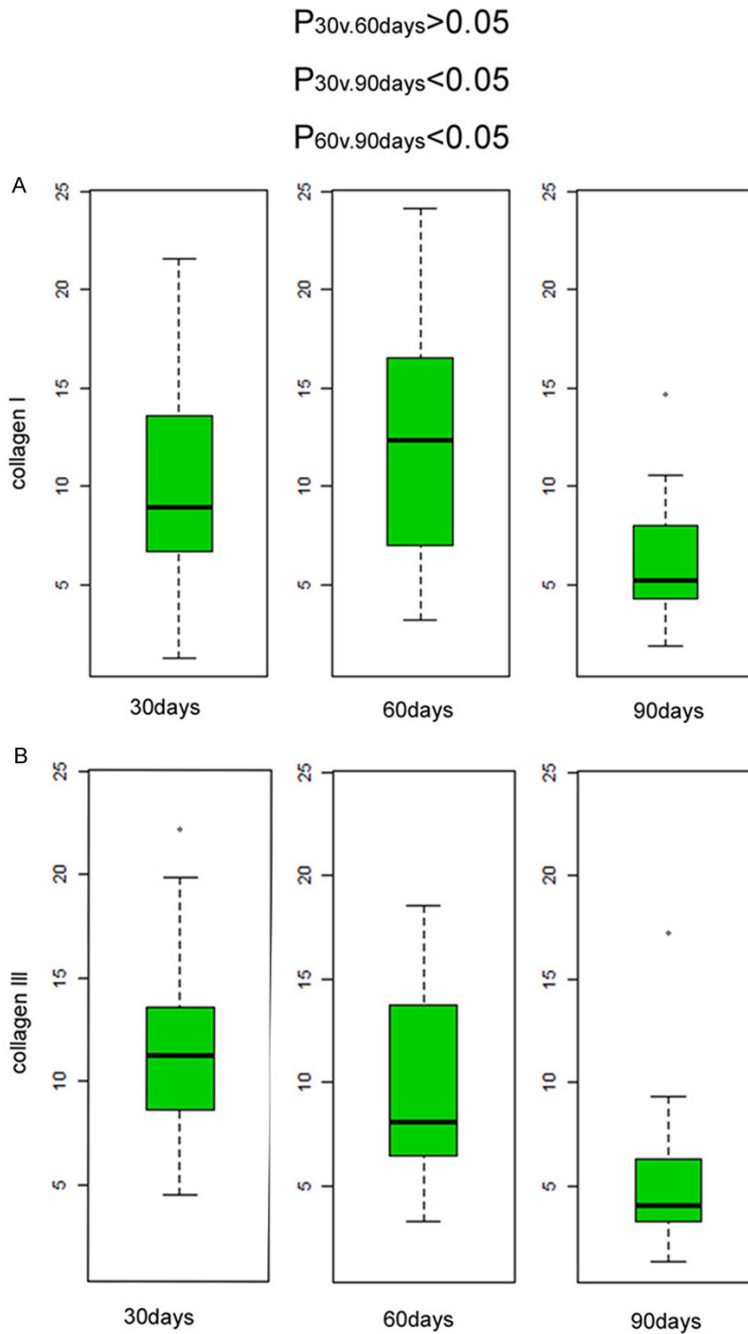


**Figure 5.** Boxplot comparison of area percentages of Picric acid-Sirius red stained collagen (type I, III) at different time periods. Collagen I (A), collagen III (B). Multiple comparisons and tests of differences between groups, respectively.

quantitative examination method. The biggest drawback is that it is difficult to achieve the same pressure applied by the operator each time [18], which in turn leads to the relative elastic contrast between the lesion and surrounding normal tissues, rather than an intrinsic parameter of tissue hardness. ARFI tech-

nology, also known as touch organization quantitative technique, implies the use of ultrasonic transducer for ROI launch. This is focused on the acoustic radiation force impulse, making certain parts and tissues of tiny deformation of transverse shear wave. It then uses the same ultrasonic probe to track beams at different time points, tracking and monitoring the response signal, as well as collecting and analyzing this information. Thus, it finally calculates the SWV and the degree of flexibility, reflecting regional organizations [19]. In Lee's observation of skin sclerosis [20], ARFI and SWE examination results suggested that the hardness of diseased dermis was greater, compared to normal healthy dermis, while the sensitivity of SWE was better than that of ARFI in distinguishing normal and hardened skin. In addition, the size of ARFI sampling frame is fixed and cannot be adjusted [21]. Compared with HS of rabbit ears and other thin tissue samples, the size of ARFI sampling frame is too large to affect the accuracy of measurement.

Unlike SE and ARFI, SWE is a safe acoustic radiation pulse emitted by the probe. Continuous focusing at different depths of the tissues causes the tissue particles to vibrate and generate transverse shear waves. Shear wave velocity of the detected tissues

can be accurately and quantitatively measured. Next, Young's modulus values reflect elastic changes of the tissues. These can be directly obtained to achieve the purpose of quantitative diagnosis ( $E = 3\rho c^2$ , unit: kPa,  $E$  is Young's modulus,  $c$  is shear wave velocity,  $\rho$  is tissue density). Young's modulus is positively corre-

## Shear wave elastography in HS

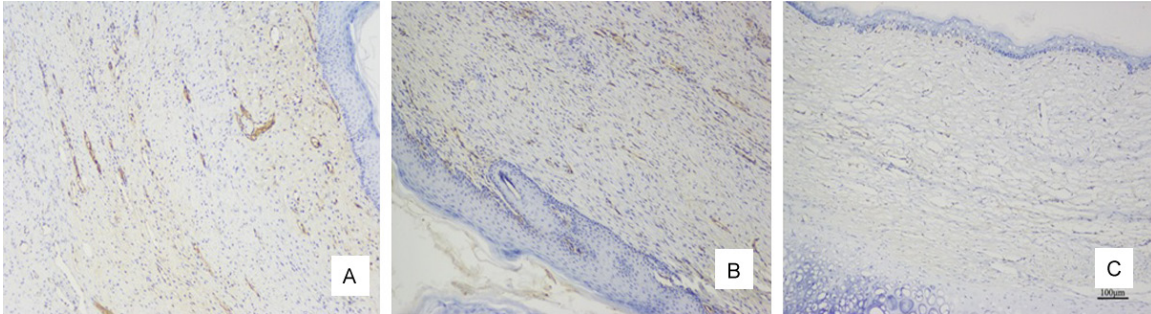


**Figure 6.** Immunohistochemistry sections at different time periods. (A) 30 days after surgery (CD34  $\times$  100); (B) 60 days after surgery (CD34  $\times$  100); (C) 90 days after surgery (CD34  $\times$  100).

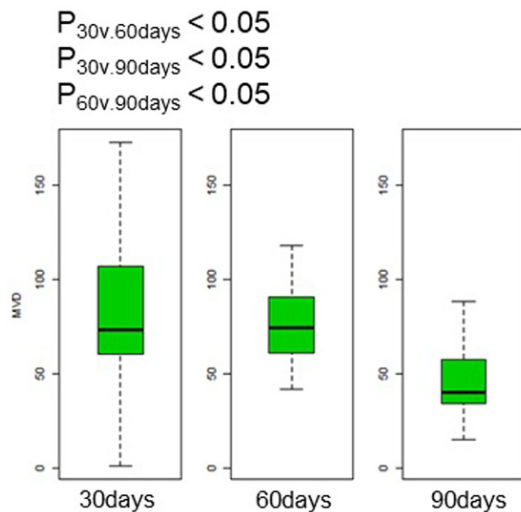


**Figure 7.** Boxplot comparisons of microvascular density by immunohistochemistry at different time points. Multiple comparisons and tests of differences between groups, respectively.

lated with tissue stiffness, with smaller E values indicating softer tissues. This new USE technology only requires the assistance of an ultrasonic probe without external pressure. It can be used to objectively and quantitatively evaluate tissue elasticity, providing more tissue information than HFUS and other USE. Thus, this method avoids the shortcomings of traditional external pressure USE, such as subjective experience and lack of objective quantitative indicators [22, 23]. It has been widely used in studies concerning the liver, breasts, prostate, thyroid, and musculoskeletal diseases [24, 28]. However, it is rarely used to study skin scars. In recent years, the French Aixplorer ShearWave™ real-time SWE ultrasonic diagnostic instrument was produced. Based on the automatic generation and analysis of real-time shear waves, Young's modulus values, which

are important biomechanical parameters, were obtained through the quantitative analysis system. The aim was to achieve full quantitative USE and promote extensive clinical research of SWE [29].

It has been reported that SWE can be used to measure skin elasticity, quantify the degree of skin fibrosis [30, 32], obtain high reliability, good repeatability, and distinguish different stages of disease [33]. These studies have laid a foundation for the application of SWE in the diagnosis and evaluation of other skin diseases.

The current study found that ventral wounds on rabbit ears produce a process of dermis proliferation, as with human HS. Previous studies have proven that fibroblasts are the main cells in scar formation, with large amounts of collagen type I and III, an important basis for scar formation. In theory, an increase in collagen fibers would harden scar tissues [34]. In this study, HS proliferation peaked at 30 days after surgery. It can be clearly seen from the boxplot that the area percentage of type III collagen with Picric acid-Sirius red staining and MVD count reached the peak level at 30 days after the surgery, while Young's modulus values of HS at this time were also the largest. Values were significantly higher, compared to those at 60 and 90 days after surgery. Within 60 to 90 days after surgery, HS gradually subsided, revealing to be mature and stable. Collagen contents of type I and III in scar tissues were reduced, MVD counts showed a decrease in the number of micro-vessels, and corresponding Young's modulus values were also gradually reduced. Experimental results showed that the change trend of elasticity was consistent with the change trend of collagen

## Shear wave elastography in HS

**Table 2.** Multiple comparisons and tests of differences between microvascular density by immunohistochemistry groups

	differences between groups	lower confidence limit	upper confidence limit	<i>p</i>
60 days postoperatively-30 days postoperatively	-8.09	-32.58	16.40	0.71
90 days postoperatively-30 days postoperatively	-41.25	-61.25	-21.25	<0.001
90 days postoperatively-60 days postoperatively	-33.16	-57.65	-8.67	0.01

*P*<0.05 was statistically significant.

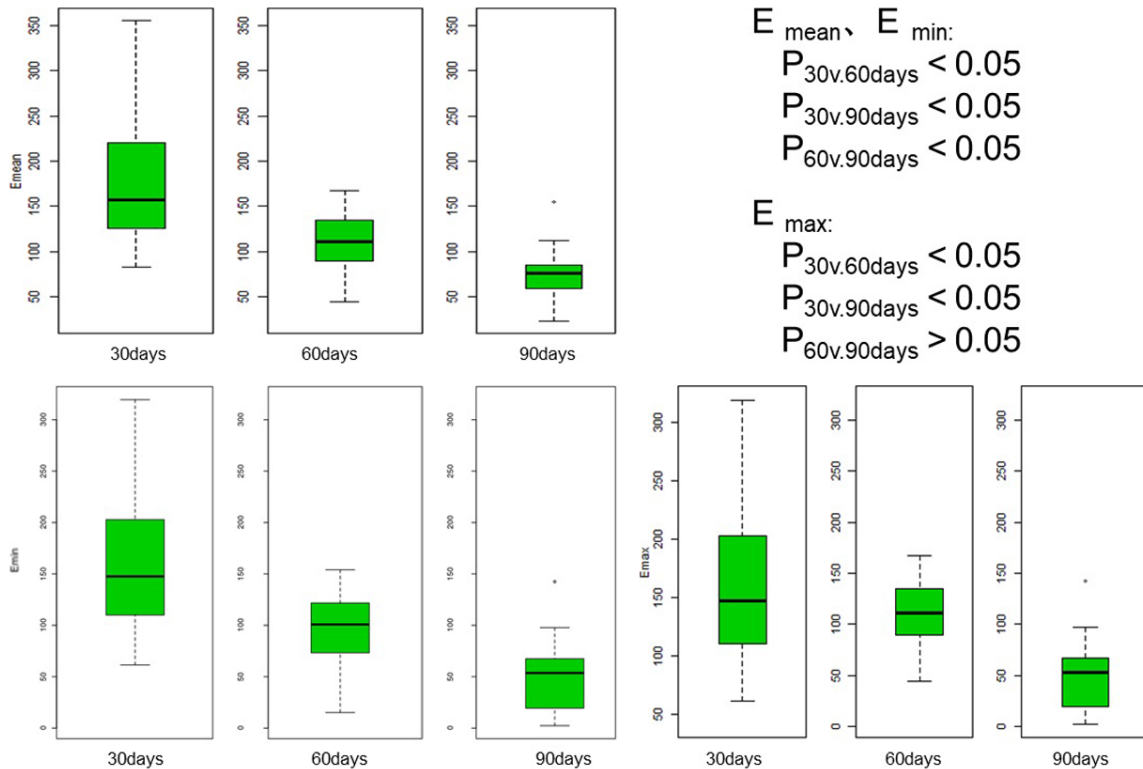


**Figure 8.** Boxplot comparisons of Young's modulus at different time points. Multiple comparisons and tests of differences between groups, respectively.

**Table 3.** Multiple comparisons and tests of differences between groups of the maximum elastic modulus

	differences between groups	lower confidence limit	upper confidence limit	<i>p</i>
60 days postoperatively-30 days postoperatively	-49.35	-73.66	-25.05	<0.001
90 days postoperatively-30 days postoperatively	-72.45	-100.51	-44.39	<0.001
90 days postoperatively-60 days postoperatively	-23.10	-54.47	8.28	0.19

*P*<0.05 was statistically significant.

content and MVD of HS. In this experiment, Young's modulus values were the largest at the peak of scar hyperplasia. Young's modulus values gradually decreased to the stage of scar resolution and maturity. This indicates

that the hardness of scar tissues in the hyperplasia stage is higher than that in the regression stage and the mature stage, consistent with Aya's [35] research results on keloids. Their results suggested that the SWV in active

## Shear wave elastography in HS

**Table 4.** Multiple comparisons and tests of differences between groups of the mean elastic modulus

	differences between groups	lower confidence limit	upper confidence limit	<i>p</i>
60 days postoperatively-30 days postoperatively	-60.80	-83.46	-38.14	<0.001
90 days postoperatively-30 days postoperatively	-96.20	-122.37	-70.04	<0.001
90 days postoperatively-60 days postoperatively	-35.40	-64.65	-6.15	0.01

*P*<0.05 was statistically significant.

**Table 5.** Multiple comparisons and tests of differences between groups of the minimum elastic modulus

	differences between groups	lower confidence limit	upper confidence limit	<i>P</i>
60 days postoperatively-30 days postoperatively	-44.30	-66.86	-21.75	<0.001
90 days postoperatively-30 days postoperatively	-105.38	-131.42	-79.33	<0.001
90 days postoperatively-60 days postoperatively	-61.07	-90.19	-31.96	<0.001

*P*<0.05 was statistically significant.

hypertrophic scar areas ( $v = 8.06$  m/s,  $v = 7.09$  m/s,  $v = 5.62$  m/s) was greater than that in mature and stable areas ( $v = 2.49$  m/s,  $v = 3.12$  m/s,  $v = 3.34$  m/s). This also confirmed that the mechanical properties of SWV were faster with stiffer tissues. However, Bhatia [36] obtained a different conclusion. He found that the hardness value of HS after surgery was relatively low. The maximum value of Stiff Pixel was 55.1 kpa, while the average value was 44.5 kpa. Therefore, it was believed that the hardness of increased fibrous tissues was not necessarily high. However, this was a case report without representativeness. Thus, their results need to be confirmed by further studies.

In the process of scar evolution, changes in collagen content and microvascular density of scar tissues are correlated with changes in Young's modulus values of scar tissues. Higher collagen content and microvascular density levels lead to greater Young's modulus values of HS. When collagen content decreases, microvascular density and Young's modulus values also decrease. Observed changes in this process suggest that changes in Young's modulus values of HS are consistent with the formation, proliferation, regression, and maturation process of scars. Thus, these values could be used to assess pathological changes of HS.

The present study, however, had a few limitations: (1) The value of HS shear wave velocity was not analyzed; and (2) The reference range

of SWE dividing HS course was not established due to small sample size.

### Conclusion

SWE can be used to dynamically and quantitatively evaluate stiffness levels of HS at different stages. Trends observed in the present study were consistent with the changes of histopathology, collagen content, and MVD in relation to the time and degree of scar evolution. Thus, SWE can be used to effectively assess the evolution of HS.

### Acknowledgements

We would like to thank Professor Shu-Guang Wu for assistance with the animal experiments.

### Disclosure of conflict of interest

None.

**Address correspondence to:** Li Qiu, Department of Ultrasound, West China Hospital of Sichuan University, No. 37, Guoxue Lane, Wuhou District, Chengdu 610041, Sichuan, China. Tel: +86-028-66000940; E-mail: wsqiuli@vip.126.com

### References

- [1] Wynn TA. Cellular and molecular mechanisms of fibrosis. *J Pathol* 2008; 214: 199-210.
- [2] Amadeu T, Braune A, Mandarim-de-Lacerda C, Porto LC, Desmoulière A and Costa A. Vascu-

## Shear wave elastography in HS

- larization pattern in hypertrophic scars and keloids: a stereological analysis. *Pathol Res Pract* 2003; 199: 469-73.
- [3] Sullivan T, Smith J, Kermode J, McIver E and Courtemanche DJ. Rating the burn scar. *J Burn Care Rehabil* 1990; 11: 256-60.
- [4] Micomonaco DC, Fung K, Mount G, Franklin J, Yoo J, Brandt M, Moore CC and Doyle PC. Development of a new visual analogue scale for the assessment of area scars. *J Otolaryngol Head Neck Surg* 2009; 38: 77-89.
- [5] Kreuter A. Localized scleroderma. *Dermatol Ther* 2012; 25: 135-47.
- [6] Iyengar S, Makin IR, Sadhwani D, Moon E, Yanes AF, Geisler A, Silapunt S, Servaes S, Weil A, Poon E and Alam M. Utility of a high-resolution superficial diagnostic ultrasound system for assessing skin thickness: a cross-sectional study. *Dermatol Surg* 2018; 44: 855-864.
- [7] Kaiser M, Yafi A, Cinat M, Choi B and Durkin AJ. Noninvasive assessment of burn wound severity using optical technology: a review of current and future modalities. *Burns* 2011; 37: 377-86.
- [8] Bamber J, Cosgrove D, Dietrich CF, Fromageau J, Bojunga J, Calliada F, Cantisani V, Correias JM, D'Onofrio M, Drakonaki EE, Fink M, Friedrich-Rust M, Gilja OH, Havre RF, Jenssen C, Klauser AS, Ohlinger R, Saftoiu A, Schaefer F, Sporea I and Piscaglia F. EFSUMB guidelines and recommendations on the clinical use of ultrasound elastography. Part 1: basic principles and technology. *Ultraschall Med* 2013; 34: 169-84.
- [9] Liu T, Zhou J, Yoshida EJ, Woodhouse SA, Schiff PB, Wang TJ, Lu ZF, Pile-Spellman E, Zhang P and Kutcher GJ. Quantitative ultrasonic evaluation of radiation-induced late tissue toxicity: pilot study of breast cancer radiotherapy. *Int J Radiat Oncol Biol Phys* 2010; 78: 811-20.
- [10] Bercoff J, Tanter M and Fink M. Supersonic shear imaging: a new technique for soft tissue elasticity mapping. *IEEE Trans Ultrason Ferroelectr Freq Control* 2004; 51: 396-409.
- [11] Athanasiou A, Tardivon A, Tanter M, Sigal-Zafarani B, Bercoff J, Deffieux T and Gennisson JL, Fink M and Neuenschwander S. Breast lesions: quantitative elastography with supersonic shear imaging—preliminary results. *Radiology* 2010; 256: 297-303.
- [12] Yu R, Song Y, Chen JJ, Liu XX and Cen Y. Establishment of an animal model of rabbit's ear with intermediate stage hypertrophic scar. *West China Medical Journal* 2010; 25: 1209-1212.
- [13] Simons M, Kee EG, Kimble R and Tyack Z. Ultrasound is a reproducible and valid tool for measuring scar height in children with burn scars: a cross-sectional study of the psychometric properties and utility of the ultrasound and 3D camera. *Burns* 2017; 43: 993-1001.
- [14] Song CH. Ultrasound detection of hypertrophic scar in different stage of hand scar excision for skin graft. *J Clin Ultrasound in Med* 2016; 18: 62-64.
- [15] Mo J, Xu H, Qiang B, Giambini H, Kinnick R, An KN, Chen S and Luo Z. Bias of shear wave elasticity measurements in thin layer samples and a simple correction strategy. *Springerplus* 2016; 5: 1341.
- [16] Nowicki A and Dobruch-Sobczak K. Introduction to ultrasound elastography. *J Ultrason* 2016; 16: 113-24.
- [17] Aya R, Yamawaki S, Muneuchi G, Naitoh M and Suzuki S. Ultrasound elastography to evaluate keloids. *Plast Reconstr Surg Glob Open* 2014; 2: e106.
- [18] Carlsen JF, Ewertsen C, Lönn L and Nielsen MB. Strain elastography ultrasound: an overview with emphasis on breast cancer diagnosis. *Diagnostics (Basel)* 2013; 3: 117-25.
- [19] Cui GH, Yang Z, Sun F, You CL and Zhang WX. Discussion on influence factors of acoustic radiation force impulse in animal models. *China Medical Devices* 2012; 27: 141-142.
- [20] Lee SY, Cardones AR, Doherty J, Nightingale K and Palmeri M. Preliminary results on the feasibility of using ARFI/SWEI to assess cutaneous sclerotic diseases. *Ultrasound Med Biol* 2015; 41: 2806-19.
- [21] Santiago T, Alcacer-Pitarch B, Salvador MJ, Del Galdo F, Redmond AC and da Silva JA. A preliminary study using virtual touch imaging and quantification for the assessment of skin stiffness in systemic sclerosis. *Clin Exp Rheumatol* 2016; 34 Suppl 100: 137-141.
- [22] Li F, Guan YM, Zhang WW, Fang QM and Guo P. Progress in ultrasonic elastography and its applications. *Clinical Focus* 2016; 31: 800-804.
- [23] Berg WA, Cosgrove DO, Doré CJ, Schäfer FK, Svensson WE, Hooley RJ, Ohlinger R, Mendelson EB, Balu-Maestro C, Locatelli M, Tourasse C, Cavanaugh BC, Juhan V, Stavros AT, Tardivon A, Gay J, Henry JP and Cohen-Bacrie C; BE1 Investigators. Shear-wave elastography improves the specificity of breast US: the BE1 multinational study of 939 masses. *Radiology* 2012; 262: 435-49.
- [24] Nikhil S, Gopu RB, Rathana CJ, Srijith K, Srijaya S, Prasanth KS, Shanid A and Devadas K. *J Clin Exp Hepatol* 2016; 6: 78-79.
- [25] Chamming's F, Mesurole B, Antonescu R, Aldis A, Kao E, Thériault M, Omeroglu A, Pinel-Giroux F, Seidler M, Solorzano S, Reinhold C and Galix B. Value of shear wave elastography for the differentiation of benign and malignant microcalcifications of the breast. *AJR Am J Roentgenol* 2019; 213: W85-W92.

## Shear wave elastography in HS

- [26] Woo S, Kim SY, Lee MS, Cho JY and Kim SH. Shear wave elastography assessment in the prostate: an intraobserver reproducibility study. *Clin Imaging* 2015; 39: 484-7.
- [27] Xu HX, Yan K, Liu BJ, Liu WY, Tang LN, Zhou Q, Wu JY, Xue ES, Shen B, Tang Q, Chen Q, Xue HY, Li YJ, Guo J, Wang B, Li F, Yan CY, Li QS, Wang YQ, Zhang W, Wu CJ, Yu WH and Zhou SJ. Guidelines and recommendations on the clinical use of shear wave elastography for evaluating thyroid nodule1. *Clin Hemorheol Microcirc* 2019; 72: 39-60.
- [28] Nicholls J, Alfuraih AM, Hensor EMA and Robinson P. Inter- and intra-reader reproducibility of shear wave elastography measurements for musculoskeletal soft tissue masses. *Skeletal Radiol* 2020; 49: 779-786.
- [29] Wang YC, Xiao HS, Xu F, Yin HQ, Gao DW and Ren YJ. Application of real time shear wave elastography in skeletal muscle system. *Chinese Journal of Medical Imaging* 2016; 238-240.
- [30] Anupam W, Abhra CC, Namita M, Saumya RT, Durga PM and Vikas A. Assessment of extent of skin involvement in scleroderma using shear wave elastography. *Indian Journal of Rheumatology* 2017; 12:194-198.
- [31] Liu H, Hou Y, Zhu QL, Xu D, Wang L, Li JC, Jiang YX, Wang Q, Li MT, Zhang FC and Zeng XF. A preliminary study of skin ultrasound in diffuse cutaneous systemic sclerosis: does skin echogenicity matter? *PLoS One* 2017; 12: e0174481.
- [32] Luo CC, Qian LX, Li GY, Jiang Y, Liang S and Cao Y. Determining the in vivo elastic properties of dermis layer of human skin using the super-sonic shear imaging technique and inverse analysis. *Med Phys* 2015; 42: 4106-15.
- [33] Wang L, Yan F, Yang Y, Xiang X and Qiu L. Quantitative assessment of skin stiffness in localized scleroderma using ultrasound shear-wave elastography. *Ultrasound Med Biol* 2017; 43: 1339-1347.
- [34] Ferraioli G, Tinelli C, Lissandrin R, Zicchetti M, Bernuzzi S, Salvaneschi L and Filice C; Elastography Study Group. Ultrasound point shear wave elastography assessment of liver and spleen stiffness: effect of training on repeatability of measurements. *Eur Radiol* 2014; 24: 1283-9.
- [35] Aya R, Yamawaki S, Yoshikawa K, Katayama Y, Enoshiri T, Naitoh M and Suzuki S. The shear wave velocity on elastography correlates with the clinical symptoms and histopathological features of keloids. *Plast Reconstr Surg Glob Open* 2015; 3: e464.
- [36] Bhatia KS, Yuen EH, Cho CC, Tong CS, Lee YY and Ahuja AT. A pilot study evaluating real-time shear wave ultrasound elastography of miscellaneous non-nodal neck masses in a routine head and neck ultrasound clinic. *Ultrasound Med Biol* 2012; 38: 933-42.